Programmable Bulk Modulus in Acoustic Metamaterials Composed of Strongly Interacting Active Cells

Dylan A. Kovacevich[1] and Bogdan-Ioan Popa[1]

Department of Mechanical Engineering, University of Michigan, Ann Arbor, Michigan 48109, USA

(*Electronic mail: bipopa@umich.edu)

(Dated: 21 July 2022)

Active acoustic metamaterials are one path to acoustic properties difficult to realize with passive structures, especially for broadband applications. Here, we experimentally demonstrate a 2D metamaterial composed of coupled sensor-driver unit cells with effective bulk modulus (κ_{eff}) precisely tunable through adjustments of the amplitude and phase of the transfer function between pairs of sensors and drivers present in each cell. This work adopts the concepts of our previous theoretical study on polarized sources to realize acoustic metamaterials in which the active unit cells are strongly interacting with each other. To demonstrate the capability of our active metamaterial to produce on-demand negative, fractional, and large κ_{eff}, we matched the scattered field from an incident pulse measured in a 2D waveguide with the sound scattered by equivalent continuous materials obtained in numerical simulations. Our approach benefits from being highly scalable, as the unit cells are independently controlled and any number of them can be arranged to form arbitrary geometries without added computational complexity.

Acoustic metamaterials expand the accessible acoustic properties beyond what is offered by conventional materials, enabling enhanced wave manipulation. One strong motivator for improving our capacity in this domain is the impressive devices derived from transformation acoustics, which require extreme properties and steep gradients[1–3]. Numerous passive metamaterial unit cells have been designed that leverage resonant behavior to exhibit bulk moduli and mass densities far from those of their constituent materials, even into the negative regime[4,5]. Additionally, techniques involving the modification of feature dimension and orientation have been used to produce spatially varying and anisotropic properties[6–9]. However, the passive metamaterial design paradigm thus far has some major limitations. Given a set of property specifications, there is no clear procedure for fabricating a cohesive metamaterial from the catalog of archetypal unit cells. For example, placing resonating unit cells in close proximity changes the acoustic properties of these resonators due to their mutual near-field coupling, which suggests that each cell needs to be redesigned depending on the metamaterial geometry. Moreover, relying on resonance restricts operation to narrow frequency bands not suitable for typical engineering applications.

Active metamaterials, specifically those that are programmable and generate a coherent response to an impinging wave, are a promising alternative[10–26]. Because active metamaterials derive their functionality from electronics/computation between sensor and driver components rather than a static physical structure, they have great flexibility in operation and achievable properties. One approach to programming active unit cells is by feedback control[10–16]. This has been very successful, but there are some disadvantages associated with a controls approach, such as delays that reduce bandwidth, stability restrictions, and challenges in scalability.

In our work, we focus on active metamaterials founded on a polarized source-driven model of the acoustic behavior of materials, such as that detailed by Sieck et al.[27]. Unit cells of this type are configured to sense the local pressure or particle velocity and act as proportional monopole or dipole sources[17–22]. We refer to these as sensor-driver unit cells and their programmed transfer function as the sensor-driver gain. Each unit cell has independent behavior and resultant properties, so in theory, any number of them can be arranged to form a metamaterial of arbitrary geometry and scale. For an ideal realization, the properties of the metamaterial could be prescribed in both time/frequency and space by simply adjusting each cell's sensor-driver gain.

Experimental realizations of these sensor-driver metamaterials have demonstrated adjustable effective bulk modulus[17], mass density[17], Willis coupling parameters[20,21], non-reciprocal behavior[18,21], and anomalous reflection[22]. However, these studies were limited to a single unit cell[17,18] or an arrangement of a few non-interacting cells[19–22] because the implications of the near field effects on neighboring cells were not well understood. Additionally, the presented sensor-driver gains were typically chosen iteratively to achieve a specific result rather than by a clear procedure that would enable precise tuning. The effective properties, when determined through a two-port scattering matrix characterization, were complex and variable across the investigated frequency range with hard to control loss and gain bands. One more active metamaterial approach, which shares many characteristics with sensor-driver metamaterials, are known as virtualized meta-atoms[23–26]. These are programmed via a convolution kernel to tailor the unit cell response, and like sensor-driver metamaterials, have only been realized in limited geometries (1D waveguide and up to three cells).

Motivated by the shortcomings of existing active metamaterials, we recently developed a theory on the design and effective properties of a bulk medium composed of interacting polarized sources, which are the model for sensor-driver unit cells[28]. In that work, we represented the scattering from a homogenized medium of periodically arranged fluid cylinders with the response of identically arranged monopole and dipole sources. The amplitudes of these sources were set as proportional to the local acoustic field. The factor of proportionality (polarizability) for each source, which becomes the sensor-driver gain in a physical realization, depends on the material properties of the cylinder that the source represents. We found closed-form expressions for how the cylinder effective bulk modulus relates to the monopole polarizability and the effective mass density relates to the dipole polarizability. In a physical active metamaterial, these expressions will provide the sensor-driver gains necessary to realize desired effective properties. Because each unit cell represents a fluid cylinder, they are programmable independent of neighboring cells and can interact with each other just as the scattering from one cylinder would impinge on another. However, ideally, sensors should not be influenced by drivers in the same cell because a cylinder would not be affected by its own scattering.

In this Letter, we will show how to incorporate the effects of same cell sensor-driver interactions into the general theory and will leverage these results to design and experimentally demonstrate a 2D active metamaterial of multiple interacting cells with highly tunable bulk modulus. For validation of the effective properties, the 2D scattering of the active metamaterial from an incident pulse will be compared to that of a simulated continuous material in both the time and frequency domains. The metamaterial will be programmed for several bulk moduli, including negative, fractional, and large relative to air. A benefit of active metamaterials is their ability to control the bulk modulus and mass density independently whereas in passive structures they are coupled, i.e. a large change in one typically results in changing the other as well. We demonstrate this benefit here by maintaining the same mass density as the background for all configurations.

An active unit cell capable of tuning the bulk modulus must be configured to produce a monopole response to the locally sensed pressure. This can be achieved with a single speaker and microphone pairing. Any passive response generated by supporting structure is undesirable, as it would impact both the effective bulk modulus and mass density. The former could possibly be compensated for, but to avoid this complication, we chose to embed our metamaterial in the bottom plate of a waveguide such that it does not perturb the external wave. This is shown for a single unit cell in the diagram of Fig. 1(a). In this unit cell, the local pressure sensed by the microphone is related to the speaker output by the gain g. This gain includes the built-in transfer functions of the speaker and microphone as well as a microcontroller gain of programmable amplitude and phase. The reflected and transmitted fields produced in a purely active response to an incident wave are equivalent to those of a unit cell of continuous material with some effective acoustic properties. The effective bulk modulus of the metamaterial κ_{eff} depends on g, while the relative effective mass density is constant $\rho_{\text{eff}} = 1$, namely the same as that of air.

These active unit cells can be tiled in an array of arbitrary size and geometry in the bottom plate of a 2D waveguide, as shown in Fig. 1(b). A zoom-in of a few cells shows that the pressure sensed by a unit cell microphone is the combination of the contributions of any external sources, other unit

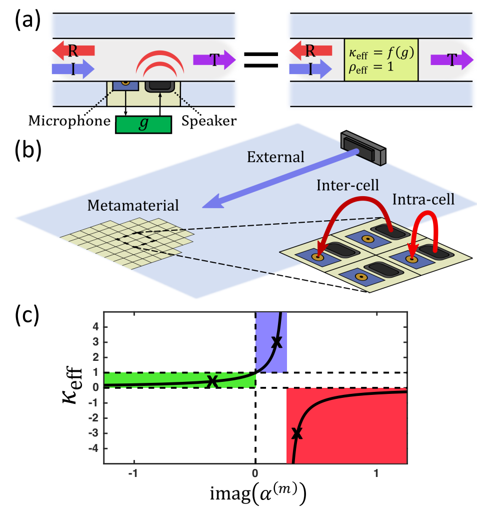

FIG. 1. (a) Equivalence of the scattered field of an active unit cell with gain g to that of a block of continuous material with bulk modulus κ_{eff}. (b) The local field sensed by an active unit cell in an array is a combination of contributions from external sources, other unit cells (inter-cell), and the driver within the same cell (intra-cell). (c) Plot of the relationship between the imaginary part of the monopole polarizability and the effective bulk modulus, distinguishing property regions of interest. Experimentally demonstrated points are marked with an x.

cell speakers (inter-cell interactions), and the speaker within the same cell (intra-cell feedback). While the inter-cell interactions are already accounted for in the polarized source model, the intra-cell feedback should also be considered in any physical realization as discussed below.

When setup in a waveguide, each unit cell speaker is modeled in the frequency domain as a line source that produces an acoustic pressure $p_s(r) = A^{(m)} H_0^{(2)}(k_0 r)$, where $A^{(m)}$ is the monopole amplitude, $H_0^{(2)}$ is the Hankel function of the second kind, k_0 is the wavenumber in the background fluid, and r is the distance from the speaker. According to theory[28], we would like to have $A^{(m)} = \alpha^{(m)} p_{\text{loc}}$, where $\alpha^{(m)}$ is the monopole polarizability and p_{loc} is the pressure sensed by the microphone excluding the intra-cell feedback. However, in reality we have $A^{(m)} = g p_m$, where p_m is the total pressure sensed by the microphone. To find the necessary open-loop gain g for the desired closed-loop gain $\alpha^{(m)}$, we analyze the closed-loop transfer function where p_{loc} is the input, $A^{(m)}$ is the output, and $H_0^{(2)}(k_0 r_m)$ is the feedback, with r_m being the distance from the speaker to the microphone. This results in the desired gain of our physical implementation as

$$g = \frac{\alpha^{(m)}}{1 + \alpha^{(m)} H_0^{(2)}(k_0 r_m)}. \quad (1)$$

From the polarized source model[28], the relationship between the monopole polarizability and the effective bulk modulus for a square array of unit cells is

$$\alpha^{(m)} = j\,(k_0 a)^2 \left(1 - \frac{1}{\kappa_{\text{eff}}}\right), \tag{2}$$

where a is half of the cell width.

Equations (1) and (2) provide direct relationships between κ_{eff} and g. Moreover, Eq. (2) gives key insight into the necessary phase of the response and the sensitivity of the bulk modulus with respect to the sensor-driver gain. A plot of the effective bulk modulus is shown in Fig. 1(c) as a function of an arbitrarily scaled imaginary $\alpha^{(m)}$, with sign emphasized by a vertical dashed line. Notably, the required phase is frequency invariant. In a real system, the phase delay will increase with frequency, causing the effective bulk modulus to deviate from the desired value. Also in Fig. 1(c), horizontal dashed lines separate the negative, positive fractional, and > 1 sections of the effective bulk modulus. Together, these lines distinguish three regions of interest in which we will demonstrate our active metamaterial's performance, with each specific κ_{eff} marked by an "x".

Fig. 1(c) shows that κ_{eff} near zero are challenging because they require greater $|\alpha^{(m)}|$ and thus greater gain g. Counterintuitively, high $|\kappa_{\text{eff}}|$ require only moderate monopole polarizabilities, but the exact value is more sensitive to variations of $\alpha^{(m)}$. These trends are parallel to those relating the amplitude of scattering from a fluid cylinder to its relative properties.

Now we return to considering the intra-cell feedback, which is neglected in the theoretical polarized source model[28]. Ideally, the microphone in one cell would be unable to sense the response of the speaker in the same cell, preventing the possibility of instability resulting from feedback. However, both hardware and software solutions to decoupling the speaker and microphone come with drawbacks. It is difficult to design a physical separating structure that does not also alter the field that the microphone should be sensing. An active control approach would require communication between unit cells and a precise model of their interactions, which would make the metamaterial no longer scalable. Instead, we chose to only employ sensor-driver gains up to a stable limit, such that there are no poles in the sensor-driver transfer function. Additionally, we used a digital bandpass filter to remove frequencies outside the band of the external excitation. Because the desired speaker response is out of phase, the range of stable gains is greater than there would be for purely positive feedback. Nonetheless, the intra-cell feedback restricts the bandwidth and accessible range of κ_{eff}. As a potential alternative route to decreasing intra-cell feedback not explored in this work, Eq. (2) shows that the polarizability magnitude required for a fixed κ_{eff} decreases with the unit cell size. This is promising if smaller cells can be manufactured and this effect is more impactful than the increase in feedback from the resultant increased proximity of the speaker and microphone within a cell.

Moving onto the actual physical implementation, a photograph of the experimental setup can be seen in Fig. 2(a), along with a zoom-in of the metamaterial in Fig. 2(b). We chose to use a 2x3 array of unit cells to form our demonstration metamaterial, outlined in red in Fig. 2(b). In this geometry, there clearly will be interactions between cells and a significant amount of scattering will be produced to differentiate between effective properties. Experiments were conducted inside a waveguide of parallel square plates of 1.2 m^2 area with a gap of 3.5 cm. A 15 cm^2 square plate containing the unit cells, each 3.7 cm^2, was fit into a cutout in the center of the bottom waveguide plate without any gaps. This allowed for the metamaterial speakers and microphones to be flush with the surface, while all other components were placed underneath, minimizing the passive response. Each unit cell was assembled in a modular style, consisting of a speaker (CUI Devices, CDS-25148), a microphone breakout board (Adafruit, SPH0645LM4H), a speaker amplifier breakout board (Adafruit, MAX98357A), and a microcontroller (PJRC, Teensy 4.0). The assemblies were externally powered through the USB port of the microcontroller and communication between the microcontroller and audio devices utilized I2S interfacing. The audio was sampled at a rate of 96 kHz and processed with an IIR elliptic bandpass filter, a number of samples delay, and a scalar gain. Each unit cell was programmed independently, so they could have had different gains and resultant properties, but we chose to demonstrate homogeneous materials for ease of interpreting the results. Custom 3D printed PLA cases for the speaker and microphone were used to press fit them into the also 3D printed metamaterial mounting plate. An external speaker at the center of the edge of the waveguide interior and oriented perpendicular to the metamaterial was used to generate the background field. This took the form of a Gaussian pulse centered at 1500 Hz and with a width of 7 periods for which

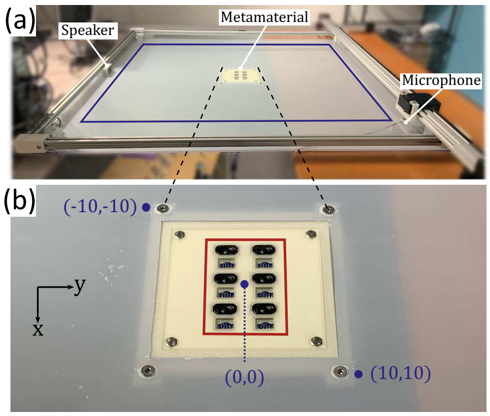

FIG. 2. (a) 2D waveguide experimental setup with the scanned measurement region outlined in blue. (b) Zoom-in of the metamaterial, outlined in red, mounted into the bottom plate of the waveguide. Sample locations for time-dependent measurement plots are marked with blue points and labeled with coordinates in cm.

the amplitude was greater than 1% of the maximum value. At this frequency, the unit cell dimension was slightly under $\lambda/6$, satisfying the subwavelength criterion. An even smaller relative cell size would be desirable, but a lower frequency was not chosen because the scattered field would be insignificant compared to the background and the wavelength too large such that waveguide edge reflections would reach the metamaterial before the trailing end of the incident pulse.

For each experiment, measurements were taken inside the waveguide in a 1 m^2 array of 2 cm resolution centered on the metamaterial. This was accomplished with a microphone magnetically affixed to the upper plate and positioned in plane with a motorized rail system. At each measurement point, ten samples were taken and averaged with the metamaterial turned off and ten with it turned on. This enabled separation of the background field, including the small passive response of the metamaterial structure, from the scattered field purely attributable to active behavior.

A comparable experimental setup was modeled in the finite element simulation software COMSOL Multiphysics, but the active metamaterial was replaced with the target equivalent continuous material. The scattering was simulated in the time and frequency domains. The background field was generated by a line source and the domain was bounded with a perfectly matched layer to prevent reflections. Samples were taken at the experimental locations and similarly processed for ease of comparison.

One method of evaluating the metamaterial performance in 2D space is by comparing the experimental and simulated scattering in the time domain at several sample locations. We chose to demonstrate this for homogeneous materials of desired $\kappa_{\text{eff}} = 3$ and $\kappa_{\text{eff}} = 0.4$. These properties were achieved in the metamaterial by programming each unit cell with the gain g prescribed by Eqs. (1) and (2). The results are shown in Fig. 3 at three locations specified by their coordinates from the center of the metamaterial in cm, labeled in Fig. 2(b). Here, a negative y-coordinate specifies a sample in the reflected region, while positive is in the transmitted region. The background waves are plotted in blue and the scattered waves in red, with the experimental lines solid and simulated dashed. The time windows of the plots were chosen to cut off reflections from the waveguide boundaries at the trailing end of the pulses. For the experimental samples, the scattered wave was shifted left one period for $\kappa_{\text{eff}} = 3$ and two periods for $\kappa_{\text{eff}} = 0.4$ to account for processing delays. This delay translates into a phase of κ_{eff} linearly varying with frequency and thus the metamaterial is moderately dispersive. Importantly, the proper phase was maintained at the nominal frequency 1500 Hz. The results as shown are in strong agreement, with some possible sources of error being the frequency dispersion, intra-cell feedback, differences in the physical components between the unit cells, and large cell size compared to the theory. On the last point, it should be noted that in our work on the polarized source model we mainly examined unit cells of dimension $\lambda/50$, yet the non-ideal experimental cells shown here still perform well at $\lambda/6$.

An alternative performance evaluation approach is to compare the amplitude and phase of the scattered fields over the

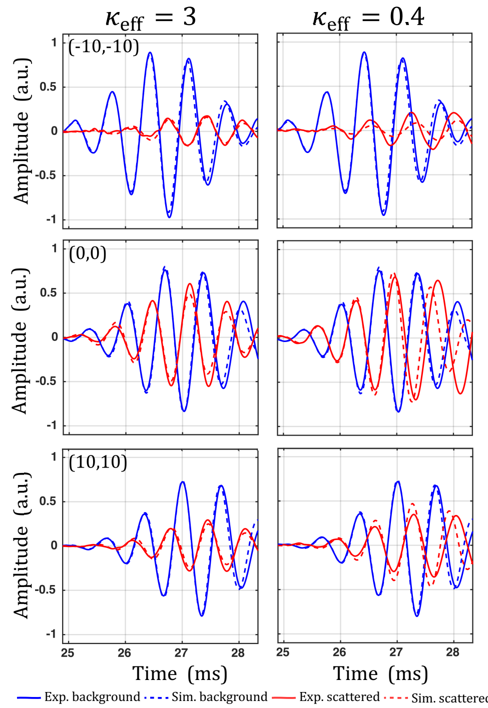

FIG. 3. Plots of the experimental background and scattered waves at several sample locations compared to simulated results with a continuous material. They are sorted in columns by effective property and in rows by location.

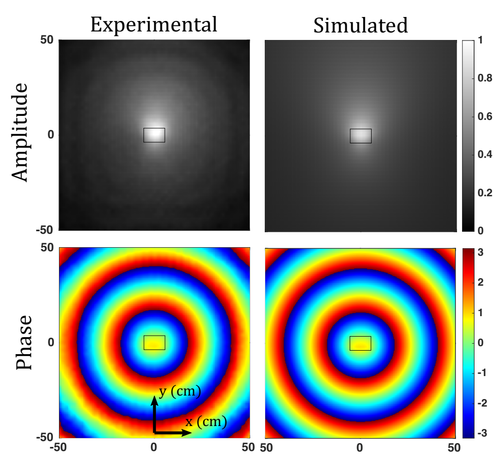

FIG. 4. Comparison of experimental scattered field amplitudes and phases to simulated results for $\kappa_{\text{eff}} = -3$ at 1500 Hz.

whole 2D waveguide domain at the pulse center frequency of 1500 Hz. Experimental and simulated plots for a test material with effective bulk modulus of $\kappa_{\text{eff}} = -3$ are shown in Fig. 4. The experimental plots were generated from the fast Fourier transform of time-windowed scan data. The trailing ends of the scattered pulses far from the metamaterial are cut off to avoid boundary reflections, resulting in a steep decrease in amplitude not indicative of the actual field. The simulations were done in the frequency domain at the center frequency and normalized by the background field at the center of the test material. It can be seen that the amplitude directivity and phases of the scattered fields are in excellent agreement.

To conclude, we have demonstrated an active metamaterial with acoustic behavior equivalent to a slab of continuous material with tunable effective bulk modulus. The metamaterial was composed of strongly interacting sensor-driver unit cells and was programmed to realize large negative, positive, as well as fractional bulk modulus. The self-contained unit cell design enabled easy adjustment of the response magnitude and phase, as well as diminished unwanted intra-cell feedback. The general architecture shown here could be scaled to a high number of cells in an arbitrary geometry, programmed to realize a material with inhomogenous bulk modulus, as well as modified to also influence the effective mass density.

This work was supported by the National Science Foundation under Grant No. CMMI-1942901.

[1]H. Chen and C. T. Chan, Applied Physics Letters **91**, 183518 (2007), publisher: American Institute of Physics.

[2]S. A. Cummer and D. Schurig, New Journal of Physics **9**, 45 (2007), publisher: IOP Publishing.

[3]A. N. Norris, Proceedings of the Royal Society A: Mathematical, Physical and Engineering Sciences **464**, 2411 (2008), publisher: Royal Society.

[4]N. Fang, D. Xi, J. Xu, M. Ambati, W. Srituravanich, C. Sun, and X. Zhang, Nature Materials **5**, 452 (2006), number: 6 Publisher: Nature Publishing Group.

[5]Z. Yang, J. Mei, M. Yang, N. H. Chan, and P. Sheng, Physical Review Letters **101**, 204301 (2008), publisher: American Physical Society.

[6]J. B. Pendry and J. Li, New Journal of Physics **10**, 115032 (2008), publisher: IOP Publishing.

[7]B.-I. Popa and S. A. Cummer, Physical Review B **80**, 174303 (2009), publisher: American Physical Society.

[8]S. Zhang, C. Xia, and N. Fang, Physical Review Letters **106**, 024301 (2011), publisher: American Physical Society.

[9]L. Zigoneanu, B.-I. Popa, and S. A. Cummer, Physical Review B **84**, 024305 (2011), publisher: American Physical Society.

[10]A. Baz, The Journal of the Acoustical Society of America **143**, 1376 (2018), publisher: Acoustical Society of America.

[11]A. Baz, Journal of Applied Physics **125**, 074503 (2019), publisher: American Institute of Physics.

[12]X. Li, Y. Chen, X. Zhang, and G. Huang, Extreme Mechanics Letters **39**, 100837 (2020).

[13]S. Raval, H. Zhou, and A. Baz, Journal of Applied Physics **129**, 074501 (2021), publisher: American Institute of Physics.

[14]H. Zhou and A. Baz, The Journal of the Acoustical Society of America **150**, 1092 (2021), publisher: Acoustical Society of America.

[15]W. Akl and A. Baz, Applied Acoustics **178**, 108001 (2021).

[16]X. Li, Y. Chen, R. Zhu, and G. Huang, Mechanical Systems and Signal Processing **149**, 107324 (2021).

[17]B.-I. Popa, L. Zigoneanu, and S. A. Cummer, Physical Review B **88**, 024303 (2013), publisher: American Physical Society.

[18]B.-I. Popa and S. A. Cummer, Nature Communications **5**, 3398 (2014), number: 1 Publisher: Nature Publishing Group.

[19]B.-I. Popa, D. Shinde, A. Konneker, and S. A. Cummer, Physical Review B **91**, 220303 (2015), publisher: American Physical Society.

[20]B.-I. Popa, Y. Zhai, and H.-S. Kwon, Nature Communications **9**, 5299 (2018), number: 1 Publisher: Nature Publishing Group.

[21]Y. Zhai, H.-S. Kwon, and B.-I. Popa, Physical Review B **99**, 220301 (2019), publisher: American Physical Society.

[22]Y. Zhai, H.-S. Kwon, and B.-I. Popa, Physical Review Applied **16**, 034023 (2021), publisher: American Physical Society.

[23]C. Cho, X. Wen, N. Park, and J. Li, Nature Communications **11**, 251 (2020), number: 1 Publisher: Nature Publishing Group.

[24]C. Cho, X. Wen, N. Park, and J. Li, Communications Physics **4**, 1 (2021), number: 1 Publisher: Nature Publishing Group.

[25]X. Wen, X. Zhu, H. W. Wu, and J. Li, Physical Review B **104**, L060304 (2021), publisher: American Physical Society.

[26]X. Wen, X. Zhu, A. Fan, W. Y. Tam, J. Zhu, H. W. Wu, F. Lemoult, M. Fink, and J. Li, Communications Physics **5**, 1 (2022), number: 1 Publisher: Nature Publishing Group.

[27]C. F. Sieck, A. Alù, and M. R. Haberman, Physical Review B **96**, 104303 (2017), publisher: American Physical Society.

[28]D. A. Kovacevich and B.-I. Popa, Physical Review B **104**, 134304 (2021), publisher: American Physical Society.

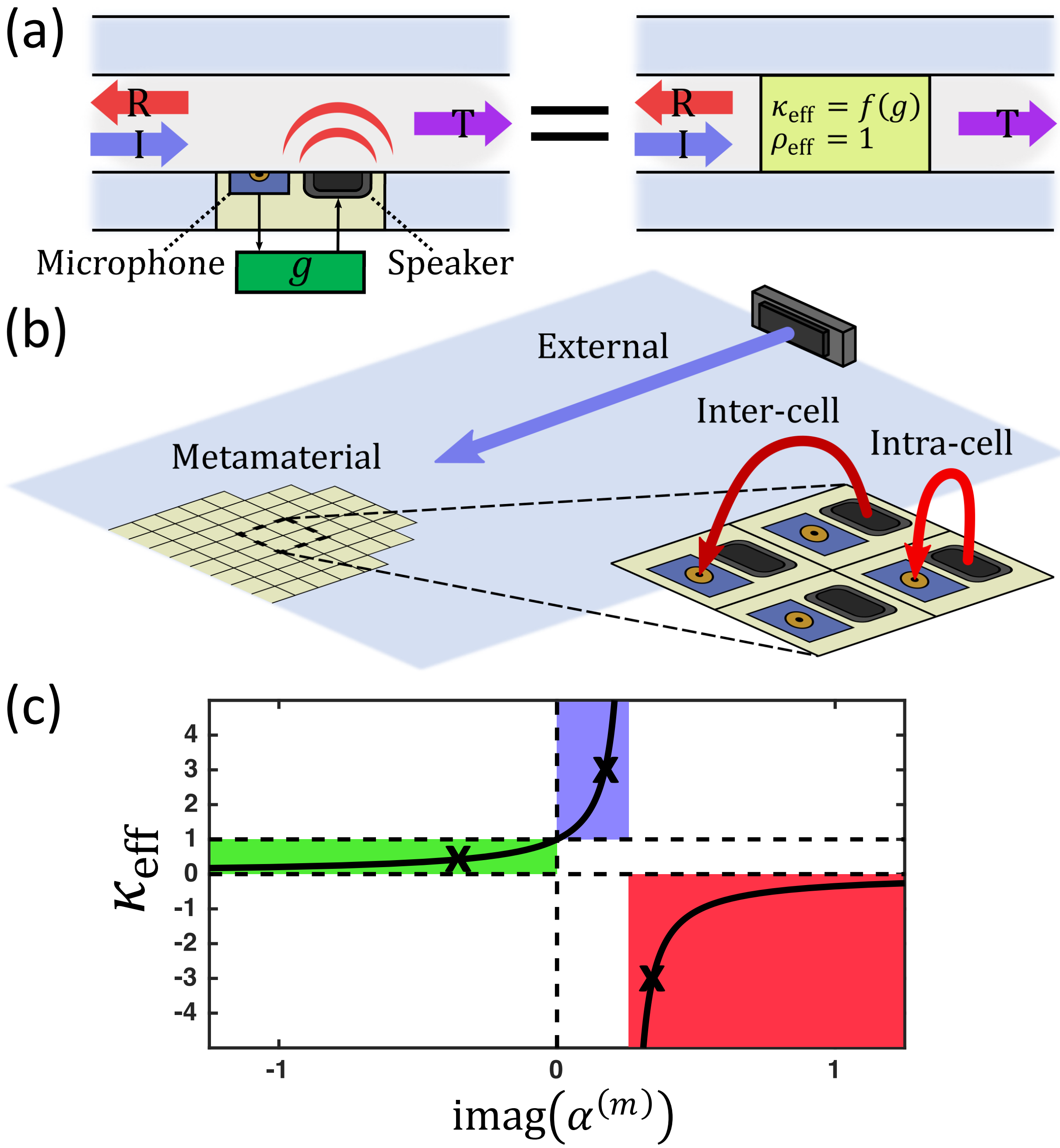
(a)
R
I
T
Microphone
g
Speaker
=
R
I
$\kappa_{\text{eff}} = f(g)$
$\rho_{\text{eff}} = 1$
T
(b)
External
Inter-cell
Intra-cell
Metamaterial
(c)
κ_{eff}
4
3
2
1
0
-1
-2
-3
-4
-1
0
1
$\text{imag}(\alpha^{(m)})$

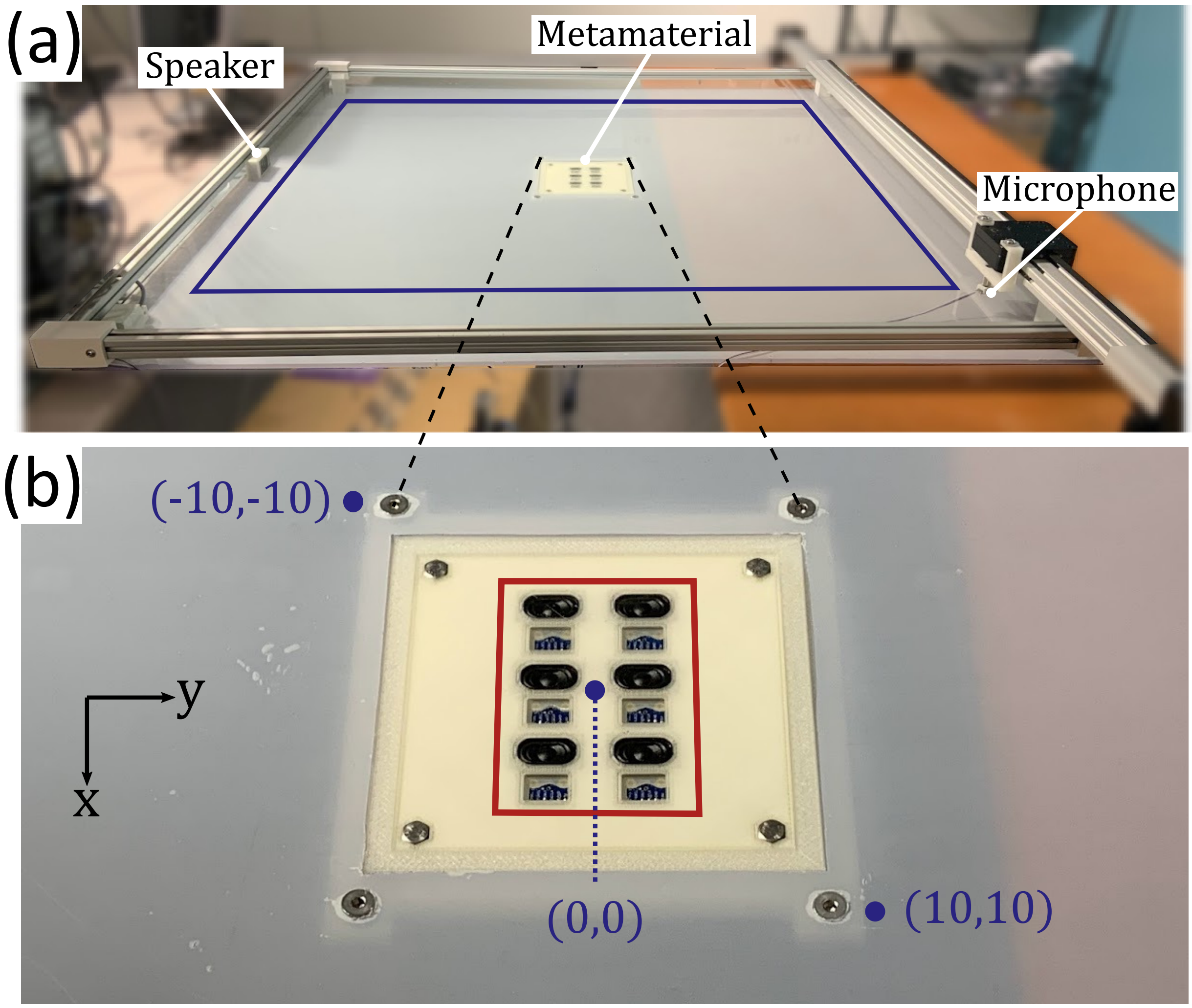
(a)
Speaker
Metamaterial
Microphone
(b)
(-10,-10)
y
x
(0,0)
(10,10)

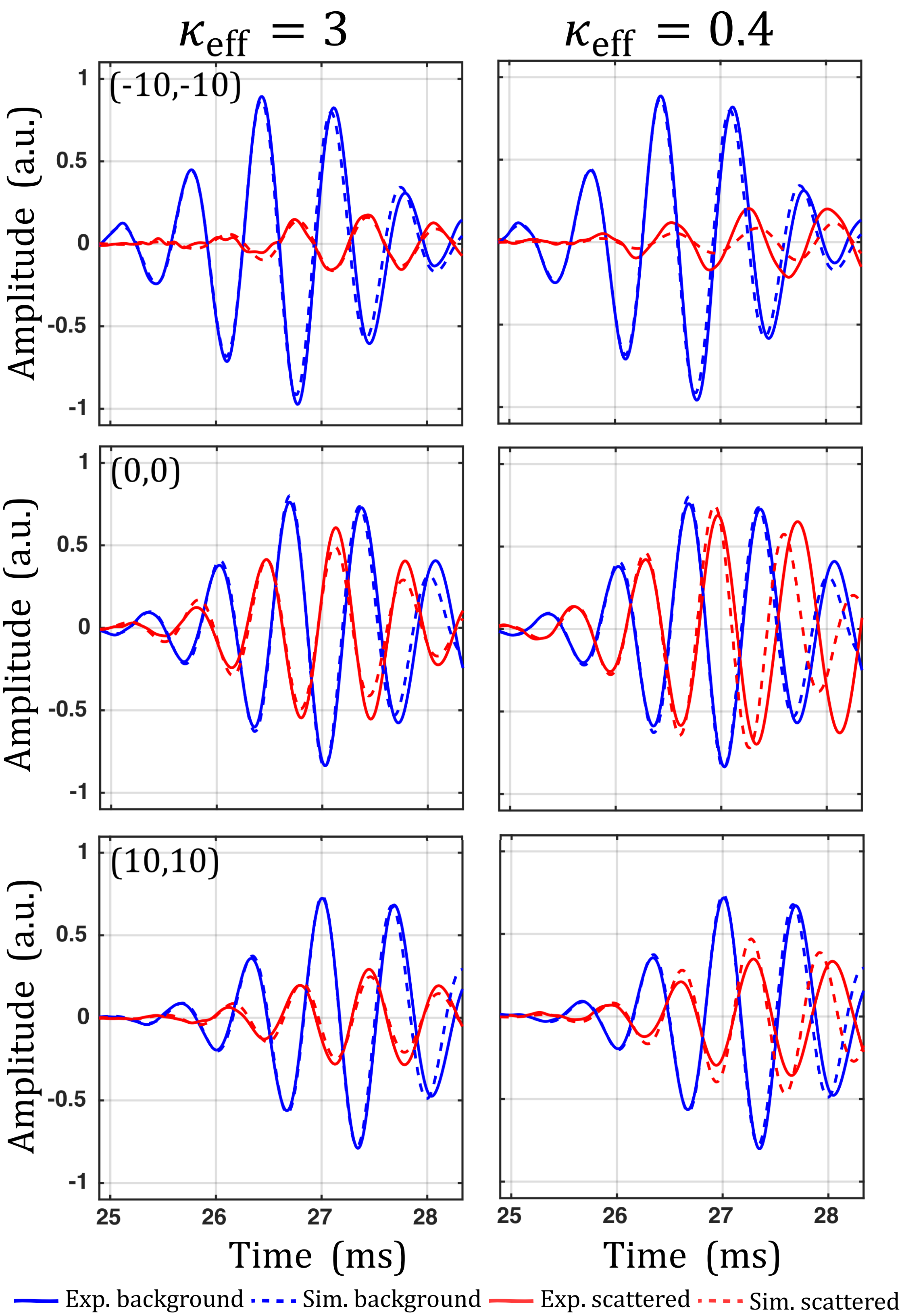
$\kappa_{\rm eff}$ = 3
$\kappa_{\rm eff}$ = 0.4
(-10,-10)
(0,0)
(10,10)
Amplitude (a.u.)
1
0.5
0
-0.5
-1
25
26
27
28
Time (ms)
Exp. background
Sim. background
Exp. scattered
Sim. scattered

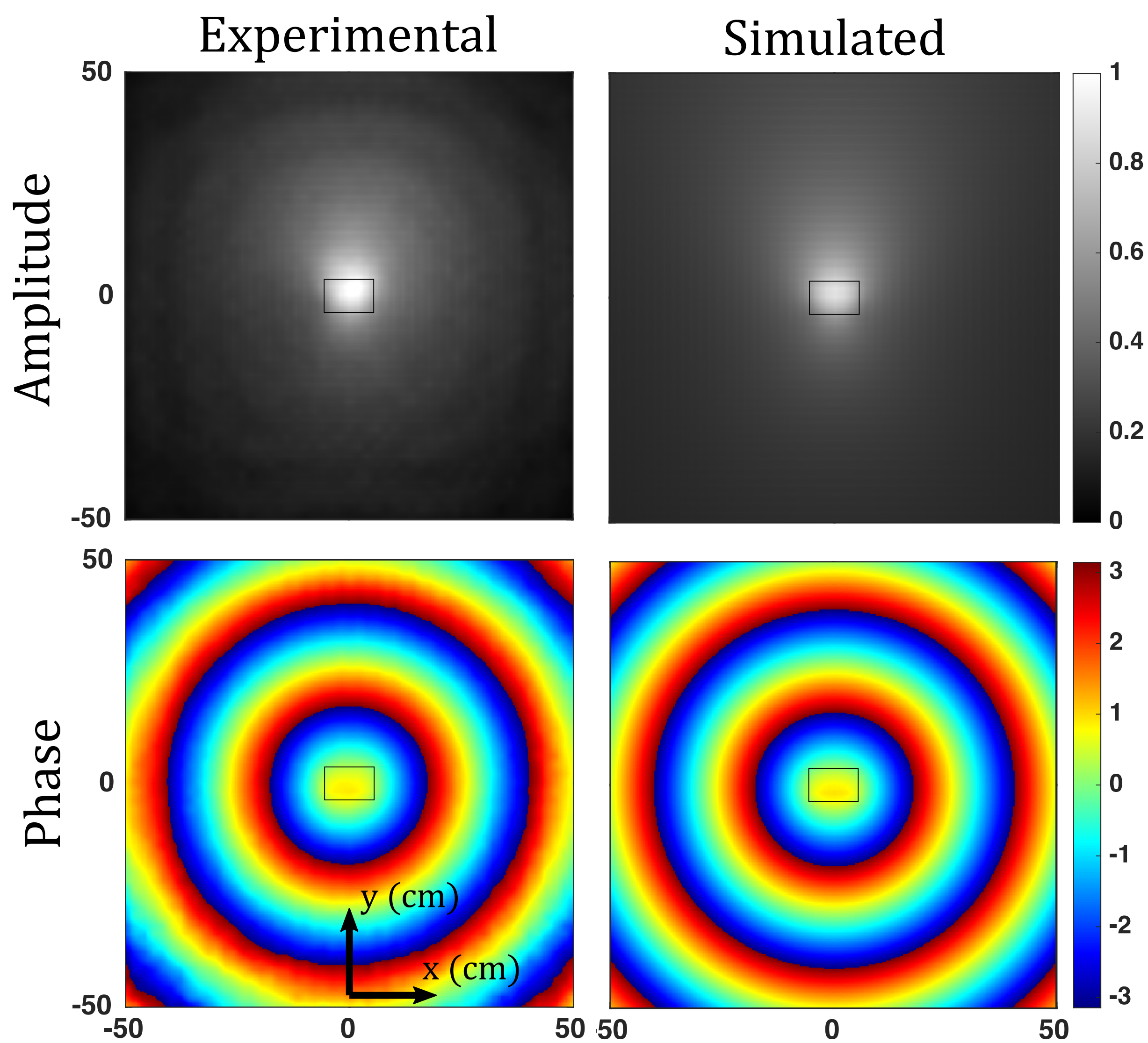
Experimental
Simulated
Amplitude
Phase
y (cm)
x (cm)
50
0
-50
-50
0
50
50
0
50
1
0.8
0.6
0.4
0.2
0
3
2
1
0
-1
-2
-3